IEEE Access
Multidisciplinary | Rapid Review | Open Access Journal

Received May 26, 2021, accepted May 28, 2021, date of publication June 3, 2021, date of current version June 10, 2021.

Digital Object Identifier 10.1109/ACCESS.2021.3085585

Imbalance Compensation of the Grid Current Using Effective and Reactive Power for Split DC-Link Capacitor 3-Leg Inverter

SUN-PIL KIM[1], SUNG-GEUN SONG[1], (Member, IEEE), SUNG-JUN PARK[2], AND FEEL-SOON KANG[3], (Member, IEEE)

[1]Energy Conversion Research Centre, Korea Electronics Technology Institute, Gwangju 61011, South Korea
[2]Department of Electrical Engineering, Chonnam National University, Gwangju 61186, South Korea
[3]Department of Electronic Engineering, Hanbat National University, Daejeon 34158, South Korea

Corresponding author: Feel-Soon Kang (feelsoon@hanbat.ac.kr)

This work was supported in part by the Korea Institute of Energy Technology Evaluation and Planning (KETEP) Grant by the Korean Government through the Ministry of Trade, Industry and Energy (MOTIE) (Development of Demonstration Zone for New Electricity Service Model) under Grant 20194310100030, and in part by the BK21 Program by the Ministry of Education and National Research Foundation of Korea under Grant I20SS7608037.

ABSTRACT Unbalanced loads cause the imbalance of the grid current and the resulting imbalance of the grid voltage when the imbalance rate of the grid current increases considerably. To cope with this problem flexibly at low cost, we modify the circuit structure from previously installed Δ-Y transformer 3-phase 3-leg inverter to split dc-link capacitor 3-leg inverter eliminating the transformer. And then we propose two kinds of compensation algorithms for balancing the grid current that can basically utilize a preinstalled control board. It is divided into reactive compensation, where dc-link of the inverter does not supply effective power to the grid but compensates for the imbalance of grid current, and effective compensation, where dc-link of the inverter supplies effective power to the grid for compensating the unbalanced grid current. We design an additional power calculator board to obtain power information, and apply it to a 10kW prototype, and then verify its validity through PSIM simulation and experiments.

INDEX TERMS Energy storage system (ESS), power conditioning system (PCS), sinusoidal pulse width modulation (SPWM), split dc-link capacitor, 3-leg inverter, 3-phase 4-wire system, unbalanced current compensation.

I. INTRODUCTION

In 3-phase 3-wire structures, voltage imbalance cannot be avoidable as an unbalanced current when load imbalance occurs [1]–[8]. Therefore, we need to design by allocating power capacity so that single-phase and three-phase, linear and nonlinear loads are balanced. However, the originally designed power capacity will be changed by the load extension or load operation pattern, which often exceeds the allowable range of facility. The imbalance rate is increasing significantly due to various single-phase loads or nonlinear loads. This can cause a number of problems on the load or the grid, such as a drop in the equipment's output power and an increase in losses, due to excessive current flow to the neutral line [9]–[11]. To alleviate this problem, the 3-leg inverter employing a Δ-Y transformer [12] and zigzag transformer [13] were introduced in low-voltage distribution networks. However, there is a significant increase in weight and cost with transformers [14]. Three single-phase H-bridges coupled to the loads with an isolation transformer was introduced for 4-wire active power filtering [15]. It needs lower dc-link voltage, which is a half as compared to split dc-link capacitor 3-leg inverter. Although this power converter requires a large number of switching devices, the output voltage is equal to the 3-level inverter resulting in better THD (total harmonic distortion) and reduced size of passive filters. Because three phases are independent to each other, when a fault in any one phase, the other two phases still work ensuring high reliability [16]. Despite the galvanic isolation and high reliability, there is a problem of increasing the volume and weight of transformers as the system power capacity increases. The way to respond to the problem of load imbalance without using a heavy and bulky transformer is to employ a type of 3-phase 4-wire inverters [8], [17]–[38].

The associate editor coordinating the review of this manuscript and approving it for publication was Ahmed Aboushady.

Split dc-link capacitor 3-leg inverter, one of the 3-phase 4-wire inverters, shows the simplest circuit configuration with the least number of switching devices. It connects the midpoint of split dc-link capacitors with the neutral point of the grid or load. Therefore, this topology acts as three single-phase half-bridge inverters, thus each leg of the inverter can be controlled independently [39] and has the advantage of being easy to implement using sinusoidal pulse width modulation (SPWM). Split dc-link capacitor 3-leg inverter can reduce the imbalance rate by allowing the unbalanced current flowing on the neutral line to flow to the mid-point of the capacitor. However, as the imbalance rate increases, the current flowing to the neutral line increases, which occurs a voltage imbalance problem in dc-link, which causes problems such as an imbalance in output voltage and an increase in the distortion and a dc component [23]–[29]. To solve the problems, 4-leg inverter can be a good alternative. The neutral line of the 4-leg inverter is connecting to the midpoint of the additional fourth leg. Although it needs additional two switches, it does not need to utilize large and expensive capacitors. Moreover, it is capable of applying the space vector pulse width modulation (SVPWM) algorithm [31]–[40], which makes switching control easy and has the advantage of high dc-link voltage utilization ratio [39]. Thus, we can say that the 4-leg inverter is the most appropriate choice to improve the imbalance problem that occurs in the grid. However, to use the 4-leg inverter, there is only a way to replace the previously installed 3-phase 3-leg inverter, which is expensive. The structure of 3-leg inverter with Δ-Y transformer can be modified to a split dc-link capacitor 3-leg inverter by connecting the mid-point of split capacitors and the neutral point of the load with an inductor, and by eliminating the transformer. Thus, despite the disadvantages of split dc-link capacitor 3-leg inverter, it can be an economical choice that can be applied to previously installed 3-phase 3-leg inverter employing a Δ-Y transformer [8], [17].

In this paper, for split dc-link capacitor 3-leg inverter modifiable from the preinstalled Δ-Y transformer 3-leg inverter and the control system, we propose two kinds of compensation algorithms that can improve the imbalance rate of the grid current using a power calculator. The proposed algorithm is divided into reactive compensation, where dc-link of the inverter does not supply effective power to the grid but compensates for the imbalance of grid current, and effective compensation, where dc-link of the inverter supplies effective power to the grid to compensate the unbalanced grid current. We use a power calculator board to obtain power information from the grid. To verify the validity and performance of the proposed approach, we implement PSIM simulations and experiments based on 10kW prototype.

II. PROPOSED IMBALANCE COMPENSATION OF THE GRID CURRENT

Under unbalanced 3-phase load conditions, the amplitude of each load current may appear differently, the amplitude is the same, but the phase angle difference may occur, or both amplitude and phase angle may appear differently. The imbalance rate of the grid voltage varies greatly depending on the operation method or pattern of the load, but the load imbalance rate is closely related to the imbalance of the grid current. Therefore, the grid-connected inverter can be used to solve the current imbalance problem by distributing the unbalanced current at the grid and to improve the power factor through controlling the reactive power.

To compensate for the unbalanced current of the grid by utilizing PCS (Power Conditioning System), it must be a structure in which the unbalanced current can flow between the neutral point of the load and the inverter.

A. SPLIT DC-LINK CAPACITOR 3-LEG INVERTER

Fig. 1 shows the circuit configuration of the 3-phase 3-leg inverter, which is connected in parallel between the grid and the unbalanced load of general electricity consumers. The unbalanced load can be consisted of 3-phase loads and single-phase loads and here they are expressed as equivalent loads (Z_x, Z_y, and Z_z). Fig. 1(a) shows a circuit configuration of 3-leg inverter employing a Δ-Y transformer. Because there is no current path via the inverter, the unbalanced current flows through the grid when the load imbalance occurs. Thus, if the imbalance rate of the load increases continuously, the grid voltage imbalance cannot be avoidable as the unbalanced current flowing through the grid. As shown in Fig 1(b), the split dc-link capacitor 3-leg inverter is a structure that can be implemented without significant modifications in the previously installed Δ-Y transformer 3-leg inverter by splitting dc-link capacitors and connecting the mid-point of the capacitor and the neutral point of the load using an inductor, and by removing the transformer. It can flow the unbalanced current through the neutral inductor. The split dc-link capacitor 3-leg inverter requires large capacitors to minimize voltage imbalance due to the unbalanced current flowing through the mid-point of the split dc link capacitors. In addition, because only up to a half of dc-link voltage is being available, it needs high dc-link voltages to apply SPWM (Sinusoidal Pulse Width Modulation). In the past, voltage utilization ratio was an important issue because of low dc-link voltage. However, modern PCSs are designed to have dc-link voltage of 700∼800V and some above 1000V. In other words, as the dc-link voltage of PCS increases, the disadvantage to the dc voltage utilization ratio of the SPWM naturally improve. In addition, ac electrolytic capacitors that make up dc-link improve the heating problem caused by ac current flowing through the mid-point.

SPWM or SVPWM can be applied to 3-phase 4-wire inverters. Generally, SVPWM is more powerful in its performance than SPWM, especially in the viewpoint of dc utilization ratio. Sometimes some researchers say SVPWM is complex in implementation of program code than SPWM, however, SVPWM just needs 4-5 lines more than SPWM in practical applications. Thus, it is better choice to use SVPWM than SPWM. However, if the grid has a problem, the inverter changes from the grid-connected mode to

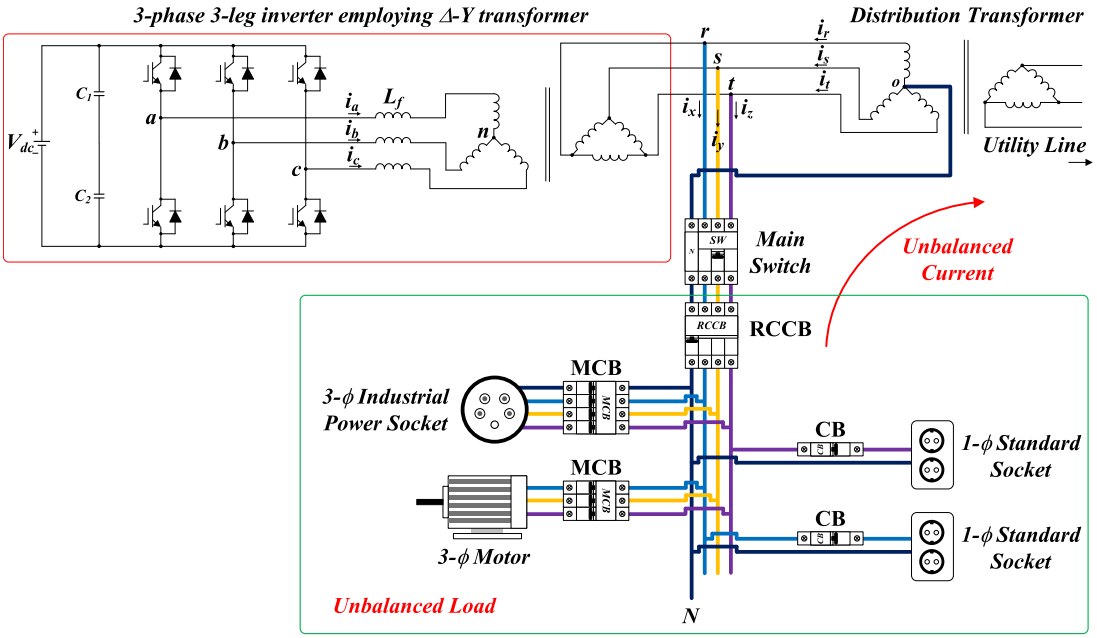

FIGURE 1. Circuit configuration of 3-phase inverter with unbalanced loads, (a) conventional 3-leg inverter employing a Δ-Y transformer with unbalanced current flowing through the grid, (b) proposed approach using split dc-link capacitor 3-leg inverter and equivalent unbalanced load.

independent operation mode. In this case, the split dc-link capacitor 3-leg inverter performs imbalance compensation to improve the imbalance rate of the output voltage. Here the switching method is based on SPWM which is making it easier to implement the algorithm given in [8] compared to other PWM techniques. Since we use the same inverter system in the grid-connected mode, SPWM technique is continuously applied although SVPWM is generally better.

B. POWER CALCULATOR

To compensate the unbalanced grid current by the proposed algorithm, power information is required at the point where the inverter is connected in parallel. Since most of the previously installed 3-leg inverters detect and control only the output voltage and output current of the inverter, thus information for the grid and the load is obtained by using an additional measurement system, so called power calculator in this paper. Fig. 2 shows the internal block diagram of the power calculator. It measures voltage and current of the grid and the load, then calculates the effective and reactive power and transfers them to the previously installed controller. Each phase angle of voltage and current is calculated via PLL (Phase-Locked Loop) and they are converted into a stationary reference frame. The proposed algorithm controls each phase current of the inverter separately. Thus, we perform individual coordinate transformations on each phase current of the inverter to obtain the d-axis and q-axis values in the stationary reference frame. In the balanced 3-phase system, the grid voltage is converted into a stationary reference frame by

$$\begin{bmatrix} V_\alpha \\ V_\beta \end{bmatrix} = \frac{2}{3} \begin{bmatrix} 1 & -\frac{1}{2} & -\frac{1}{2} \\ 0 & \frac{\sqrt{3}}{2} & -\frac{\sqrt{3}}{2} \\ 1 & 1 & 1 \end{bmatrix} \begin{bmatrix} V_r \\ V_s \\ V_t \end{bmatrix} \tag{1}$$

And (1) is converted into a rotating reference frame by

$$\begin{bmatrix} V_d \\ V_q \end{bmatrix} = \begin{bmatrix} \cos\theta & \sin\theta \\ -\sin\theta & \cos\theta \end{bmatrix} \begin{bmatrix} V_\alpha \\ V_\beta \end{bmatrix} \tag{2}$$

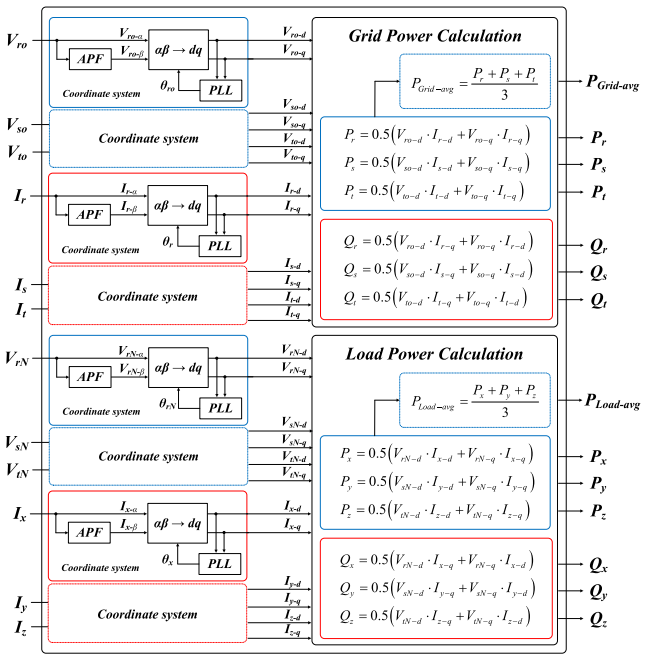

FIGURE 2. Internal block diagram of power calculator for the proposed imbalance compensation.

Thus, the balanced 3-phase voltage of the grid can be expressed as:

$$V_d = 0 \tag{3}$$
$$V_q = -V_m \tag{4}$$

where $V_\alpha = V_m \sin\omega t$ and $V_\beta = -V_m \cos\omega t$. In a balanced 3-phase condition, the d-axis is zero and the q-axis becomes the maximum value of the phase voltage. This concept is used to obtain each phase information as shown in coordinate system of Fig. 2. In the coordinate system, voltage and current of the grid and the load are transferred to the α-axis, and 90° delayed value via All-Pass-Filter (APF) is transferred to the β-axis. The voltage and current obtained by the coordinate system can be used to calculate the effective and reactive power. The effective and reactive power for the r-phase of the grid are as follows.

$$P_r = 0.5\left(V_{ro-d} \cdot I_{r-d} + V_{ro-q} \cdot I_{r-q}\right) \tag{5}$$
$$Q_r = 0.5\left(V_{ro-d} \cdot I_{r-q} + V_{ro-q} \cdot I_{r-d}\right) \tag{6}$$

The effective and reactive power for the x-phase of the load are as follows.

$$P_x = 0.5\left(V_{rN-d} \cdot I_{x-d} + V_{rN-q} \cdot I_{x-q}\right) \tag{7}$$
$$Q_x = 0.5\left(V_{rN-d} \cdot I_{x-q} + V_{rN-q} \cdot I_{x-d}\right) \tag{8}$$

The power information calculated by the power calculator is transferred to the previously installed controller of the inverter to perform the proposed compensation algorithm.

C. REACTIVE COMPENSATION ALGORITHM

The reactive compensation algorithm is a method of controlling the reactive power of each phase to zero while keeping the effective power of each phase on the grid equal. Therefore, during the inverter works with this reactive compensation algorithm, dc-link of the inverter does not supply effective power to the grid.

Fig. 3 shows the vector diagram of controlling the reactive currents (I_{a-q}, I_{b-q}, I_{c-q}) of each phase of the inverter so that when unbalanced currents (I_x, I_y, I_z) flow through the load, the grid current (I_r, I_s, I_t) becomes in phase with the phase voltage (V_{rN}, V_{sN}, V_{tN}) of the load and each phase of the grid current remains the same amplitude. Because the output voltage of the grid-connected inverter is equal to the grid voltage (V_{ro}, V_{so}, V_{to}) and the voltage applied to the load (V_{rN}, V_{sN}, V_{tN}), it is possible to control the grid current consistently through inverter reactive current control with the load phase voltage and the grid current in phase.

The reactive compensation uses the averaged effective power of the grid as follows.

$$P_{Grid-avg} = \frac{P_r + P_s + P_t}{3} \tag{9}$$

The effective power to be compensated by the inverter is as follows.

$$P_a^* = -\left(P_{Grid-avg} - P_x\right) \tag{10}$$

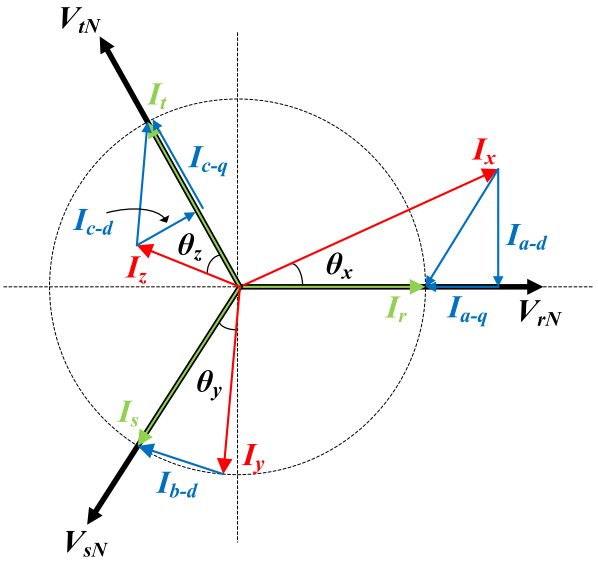

FIGURE 3. Vector diagram for compensating the imbalance of the grid current using the reactive compensation algorithm.

$$P_b^* = -\left(P_{Grid-avg} - P_y\right) \tag{11}$$
$$P_c^* = -\left(P_{Grid-avg} - P_z\right) \tag{12}$$

Here, the upper subscript asterisk (*) means the command value. The reactive power to be compensated by the inverter is as follows.

$$Q_a^* = 0 - Q_x \tag{13}$$
$$Q_b^* = 0 - Q_y \tag{14}$$
$$Q_c^* = 0 - Q_z \tag{15}$$

In (10)-(12), if there are additional power sources connected to the PCS or ESS (Energy Storage System) is charged, it shall be added to the reference command value.

$$P_a^* = -\left(P_{Grid-avg} - P_x\right) + \frac{P_{ess}}{3} + \frac{P_{offset}}{3} \tag{16}$$
$$P_b^* = -\left(P_{Grid-avg} - P_y\right) + \frac{P_{ess}}{3} + \frac{P_{offset}}{3} \tag{17}$$
$$P_c^* = -\left(P_{Grid-avg} - P_z\right) + \frac{P_{ess}}{3} + \frac{P_{offset}}{3} \tag{18}$$

Fig. 4 shows a block diagram of the reactive compensation. Fig. 4(a) produces the command value of the q-axis current in the inverter for the imbalance compensation of the grid current. The q-axis current command of the a-phase of the inverter is obtained by subtracting the effective power (P_x) of the x-phase load from the averaged grid effective power ($P_{Grid-avg}$). After adding ESS and offset power, the effective power command (P_a^*) that the a-phase of the inverter must supply is obtained. The q-axis current command (I_{a-q}^*), which is supplied by the a-phase of the inverter, is obtained by dividing P_a^* by the q-axis value of the grid voltage (V_{ro-q}) and multiplying it by -2.0. At this point, q-axis current command (I_{a-q}^*) is limited to the output current at the maximum power

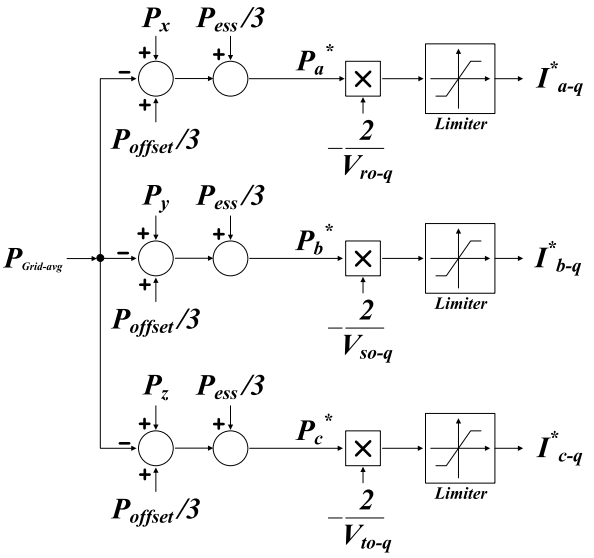

(a)

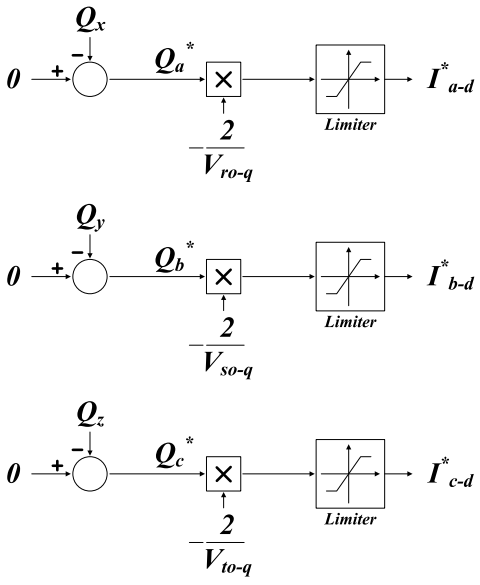

(b)

FIGURE 4. Block diagram of generating the command value of the inverter output current in reactive compensation algorithm, (a) reactive current of q-axis, (b) effective current of d-axis.

the inverter can supply.

$$I_{a-q}^* = P_a^* \times \left(-\frac{2}{V_{ro-q}}\right) \tag{19}$$
$$I_{b-q}^* = P_b^* \times \left(-\frac{2}{V_{so-q}}\right) \tag{20}$$
$$I_{c-q}^* = P_c^* \times \left(-\frac{2}{V_{to-q}}\right) \tag{21}$$

Fig. 4(b) shows a control block diagram that produces the command value of the d-axis current in the inverter. The effective current (I_{a-d}^*) of the a-phase of the inverter

is controlled so that the reactive power of the grid is zero, where the power factor is designed to compensate only in the maximum apparent power range of the inverter as (25).

$$I^*_{a-d} = -Q^*_a \times \left(-\frac{2}{V_{ro-q}}\right) \tag{22}$$

$$I^*_{b-d} = -Q^*_b \times \left(-\frac{2}{V_{so-q}}\right) \tag{23}$$

$$I^*_{c-d} = -Q^*_c \times \left(-\frac{2}{V_{to-q}}\right) \tag{24}$$

$$PF \leq \frac{\sqrt{|S_{\max}|^2 - P^2_{Inv-sum}}}{3} \tag{25}$$

D. EFFECTIVE COMPENSATION ALGORITHM

Effective compensation is a method in which the inverter directly supplies effective power to the grid to compensate unbalanced current of the grid. It requires an amplitude and phase angle information for each phase of the grid. Thus, each phase current of the grid is measured, and transformed into a synchronous coordinate system by power calculator.

Fig. 5 shows a block diagram of the effective compensation. Fig. 5(a) produces the command value of the q-axis current error. The q-axis current command error of the a-phase of the inverter is obtained by subtracting the q-axis current (I_{r-q}) of the r-phase of the grid from the q-axis component of the averaged grid current ($I_{Grid-avg-q}$). After adding the ESS charging current (I_{ess}), the q-axis command ($I^*_{a-q-error}$) is obtained. At this point, q-axis command ($I^*_{a-q-error}$) is limited to the output current at the maximum power the inverter can supply. Fig. 5(b) shows a control block diagram that produces the command value of the d-axis current in the inverter. The d-axis current (I^*_{a-d}) of the a-phase of the inverter is controlled so that the reactive power of the grid is zero, where the power factor is designed to compensate only in the maximum apparent power range of the inverter as (25). The average value of the q-axis of the grid current is as follows.

$$I_{Grid-avg-q} = \frac{I_{r-q} + I_{s-q} + I_{t-q}}{3} \tag{26}$$

As given in Fig. 5(a), the current command of the q-axis error for each phase is as follows.

$$I^*_{a-q-error} = I_{Grid-avg-q} - I_r + I_{ess} \tag{27}$$

$$I^*_{b-q-error} = I_{Grid-avg-q} - I_s + I_{ess} \tag{28}$$

$$I^*_{c-q-error} = I_{Grid-avg-q} - I_t + I_{ess} \tag{29}$$

Fig. 6 is a block diagram that adds a current compensator. To reduce the error occurring on the q-axis command value, it is compensated using the q-axis current produced by the effective power of the grid. The more the imbalance rate converges to zero, the more the output value of the compensator converges to zero. The q-axis current command value of the

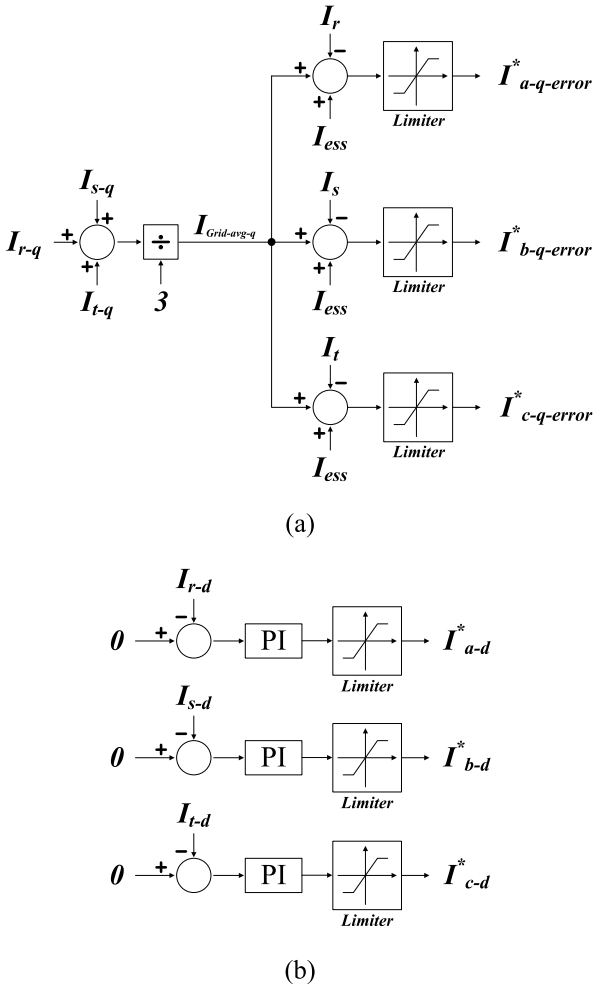

FIGURE 5. Block diagram of generating the command value of the inverter output current in effective compensation algorithm, (a) reactive current of q-axis, (b) effective current of d-axis.

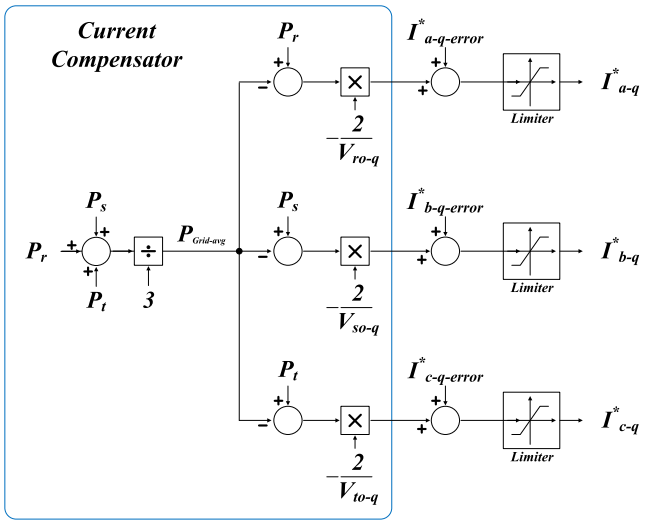

FIGURE 6. Block diagram of effective compensation algorithm with q-axis current compensator.

inverter is expressed with the current compensator as follows.

$$I^*_{a-q} = \frac{-2.0\left(P_{Grid-avg} - P_r\right)}{V_{ro-q}} + I^*_{a-q-error} \quad (30)$$

$$I^*_{b-q} = \frac{-2.0\left(P_{Grid-avg} - P_s\right)}{V_{so-q}} + I^*_{b-q-error} \quad (31)$$

$$I^*_{c-q} = \frac{-2.0\left(P_{Grid-avg} - P_t\right)}{V_{to-q}} + I^*_{c-q-error} \quad (32)$$

III. SIMULATION AND EXPERIMENT RESULTS

We validate the feasibility of the proposed compensation algorithm by PSIM simulations on the split dc-link capacitor 3-leg inverter. Table 1 shows the simulation parameters. We design controllers using C-language-based dynamic linked library (DLL) blocks. It is the same as the controller code implemented in the MCU (Micro Controller Unit) in the experiment.

TABLE 1. Simulation parameters.

Item	Values	Unit
dc-link voltage	700	V
Filter inductor	1.5	mH
Neutral line inductor	4.2	mH
dc-link capacitor*	6,800	μF
ac capacitor*	50	μF
Switching frequency	10	kHz
Power factor	0.99	PF
Imbalance rate of the load	15.69	%

*dc-link stage

Fig. 7(a) shows a simulation result before applying the imbalance compensation algorithm, and the grid voltage is balanced, but the grid current is unbalanced. The load current (rms) is x-phase 71.1A, y-phase 43.7A, and z-phase 53.7A, which is almost identical to the unbalanced current (i_r, i_s, i_t) of the grid. The output current (i_a, i_b, i_c) of the inverter is in the state where the minimum current is flowing to connect with the grid. As shown in Fig. 7(b), the sum of the grid currents is equal to the load currents. In this case, there is no current flowing through the neutral line, and the output current of the inverter are balanced.

Fig. 8(a) is a simulation result after applying the reactive compensation algorithm. The grid currents are balanced although the load currents are unbalanced. For the imbalance compensation, the inverter outputs unbalanced currents, a-phase 22.3A, b-phase 12.5A, and c-phase 11.7A in rms. When the reactive compensation is performed, the sum of the grid currents becomes almost zero, as shown in Fig. 8(b), which significantly reduces the unbalanced current. The sum of the load current and the sum of the inverter output current are equal to 26.6A (rms), indicating that the unbalanced current flows to the inverter through the neutral line. Fig. 8(c) shows the variation in effective and reactive power of the grid as the reactive compensation is applied. Before applying reactive compensation, the effective power of the

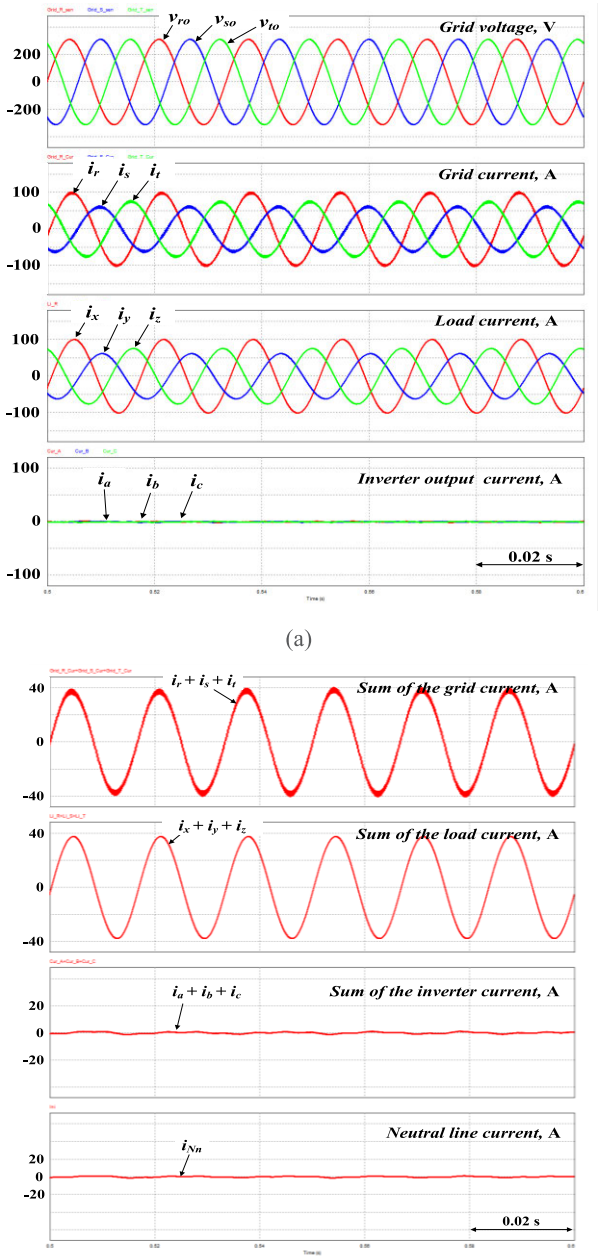

FIGURE 7. Simulation results before applying compensation algorithm, (a) Grid voltage, grid current, load current, and inverter output current, (b) Sum of the grid, load, and inverter output current.

grid is r-phase 15.1kW, s-phase 9.5kW, t-phase 11.5kW, and the reactive power is r-phase 3.0kVar, s-phase 0.3kVar, and t-phase 1.8kVar, with an imbalance rate of 15.67%. With the reactive compensation, it is shown that the effective power of each phase of the grid begins to be controlled with an average power of 12.1kW, and the reactive power becomes near to zero.

Fig. 9(a) is a simulation result after applying the effective compensation algorithm at a load imbalance rate of 15%. The grid current is balanced, and the load has an unbalanced current. The inverter outputs unbalanced currents of a-phase

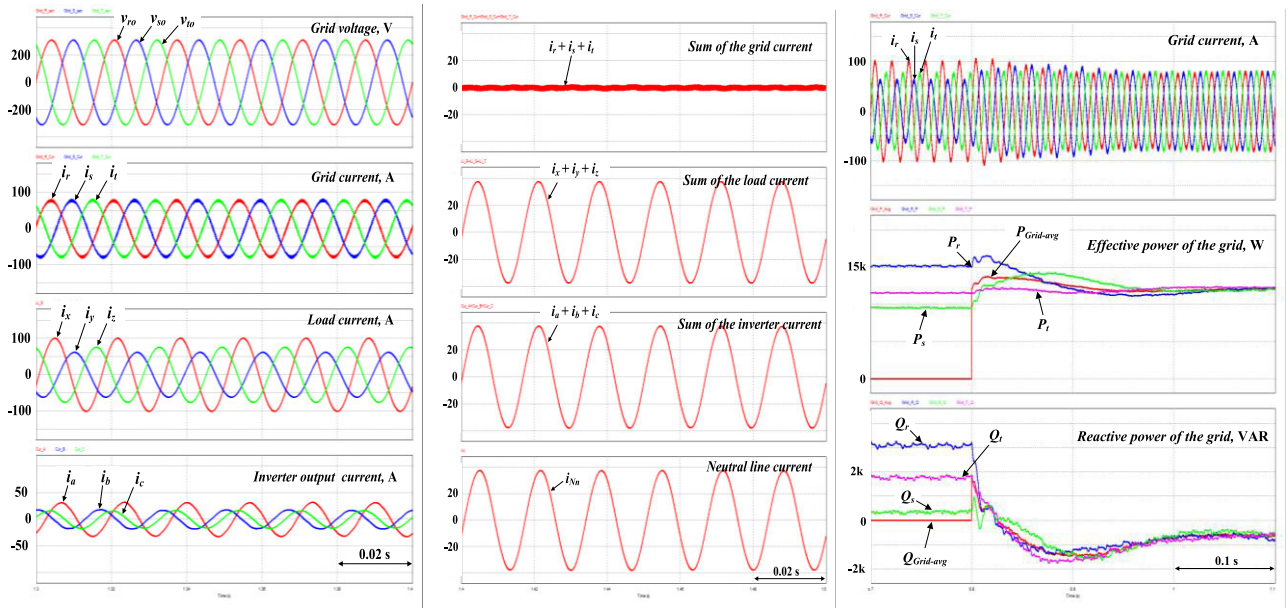

FIGURE 8. Simulation results after applying the reactive compensation, (a) Grid voltage, grid current, load current, and inverter output current, (b) Sum of the grid, load, and inverter current after applying reactive compensation, (c) Variation in effective and reactive power of the grid as the reactive compensation is applied.

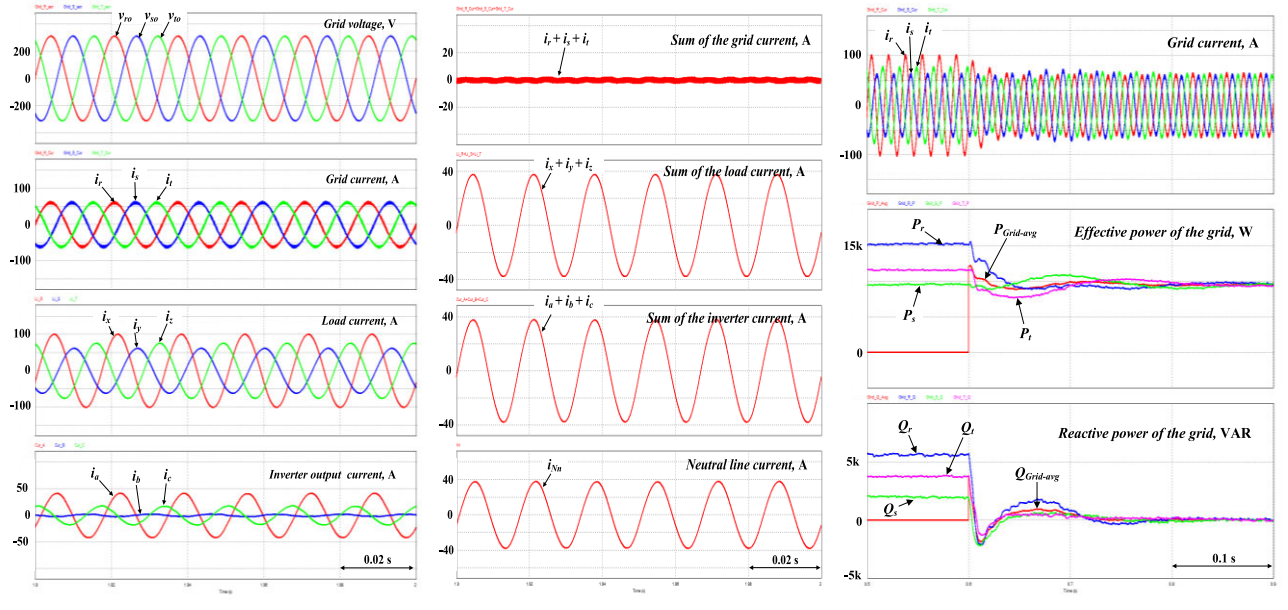

FIGURE 9. Simulation results after applying the effective compensation, (a) Grid voltage, grid current, load current, and inverter output current, (b) Sum of the grid, load, and inverter current after applying effective compensation, (c) Variation in effective and reactive power of the grid as the effective compensation is applied.

29.9A, *b*-phase 1.8A, and *c*-phase 12.9A in rms. Fig. 9(b) shows the sum of the grid currents is almost zero, indicating a significant reduction in the imbalance rate of the grid current. The unbalanced current of the load is equal to that of the inverter at 26.6A in rms. From the current waveform flowing on the neutral line, it can be seen that the unbalanced current is flowing to the inverter. Fig. 9(c) shows the effective and reactive power of the grid when applying effective compensation. The effective power of the grid before applying effective compensation is *r*-phase 15.1kW, *s*-phase 9.5kW, *t*-phase 11.5kW, and the reactive power is *r*-phase 3.0kVar, *s*-phase 0.3kVar, *t*-phase 1.8kVar, and the imbalance rate is 15.67%.

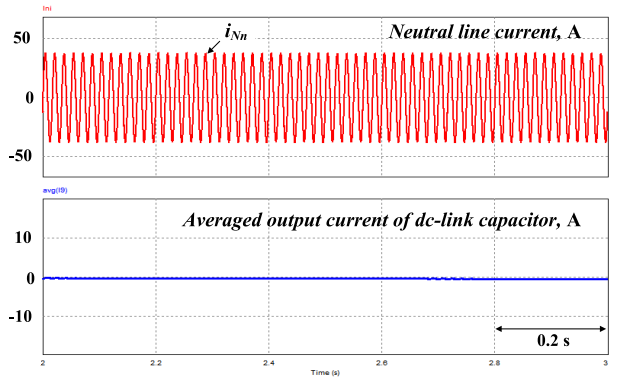

(a)

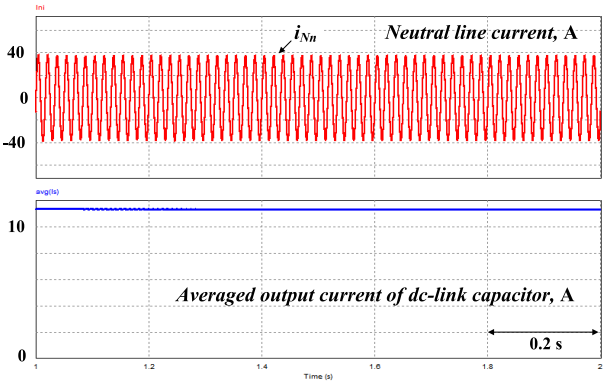

(b)

FIGURE 10. Neutral line current and averaged output current of dc-link capacitor according to the applied compensation, (a) with reactive compensation, (b) with effective compensation.

The effective compensation shows that the effective power of each phase of the grid is controlled by an average power of 9.56kW and the reactive power is almost zero.

The proposed compensation algorithms are essentially compensating for the unbalanced grid current by the inverter supplying unbalanced current. Fig. 10 shows the neutral current and the averaged output current of dc-link capacitor according to the applied compensation algorithms. Fig. 10(a) is a simulation result of applying the reactive compensation. It shows the neutral line current which means the inverter outputs unbalanced currents. The averaged output current of dc-link capacitor is almost zero. In other words, the reactive compensation does not use the dc-link energy and uses the reactive power of the grid to compensate the imbalance of the grid current. Fig. 10(b) shows a simulation result of applying the effective compensation. In order to compensate the imbalance of the grid current, the inverter supplies the effective current as much as the difference in each phase. The averaged output current of dc-link is approximately 11.5A, which shows an improvement in the imbalance rate.

For validation of the feasibility of the proposed compensation algorithms, we modify the circuit structure by adding split dc-link capacitors to the previously installed 3-leg inverter. The operating voltage range of dc-link is 650∼830V and the minimum voltage is set to 650V to apply 3-phase grid connection and the SPWM-based compensation algorithm.

Table 2 shows the specifications of the modified inverter, i.e., split dc-link capacitor 3-leg inverter used in the experiment. Fig. 11 shows a configuration of the experimental set-up with an additional power calculator board.

TABLE 2. Specifications of split dc-link capacitor 3-leg inverter for experiments.

Item	Values	Unit
Operating range of input voltage	DC 650~830	V
Maximum allowable input voltage	DC 900	V
Output power	10	kW
Output voltage	AC 380	V
Output current	20	A
Output frequency	60	Hz
Total harmonic distortion	< 2	%

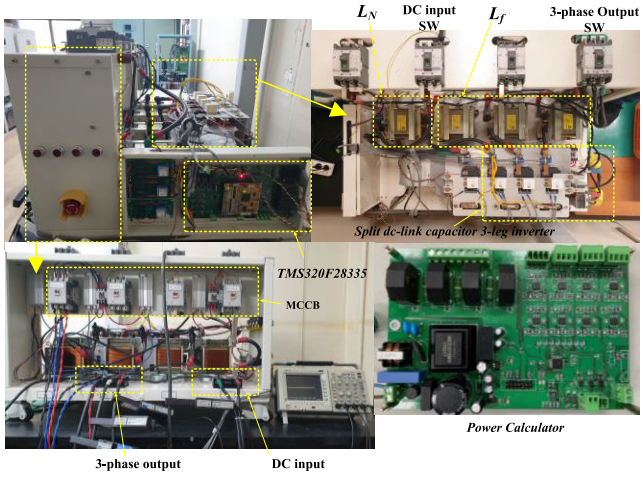

FIGURE 11. Experimental set-up with a power calculator board.

Fig. 12(a) is an experimental waveform in which the inverter outputs a balanced 3-phase current at Y-connected load of 7.8Ω each. At this time, the output current of the inverter is controlled so that d-axis is zero and q-axis is –10.0A. Then each output current of the inverter (i_a, i_b, i_c) is balanced, with a neutral line current (i_{Nn}) of nearly 0A. Fig. 12(b) is an experimental waveform when the reactive compensation algorithm is applied to compensate the imbalance of the grid current. The peak value of a-phase current (i_a) is 15.0A and the b- and c-phases (i_b and i_c) are 10.0A, respectively, indicating that each phase of the inverter outputs an unbalanced current. It can be seen that the unbalanced current flows through the neutral line (i_{Nn}) and is in-phase with the a-phase current (i_a) of the inverter. Fig. 12(c) is an experimental result when the effective compensation is applied to compensate the unbalanced grid current. The peak value

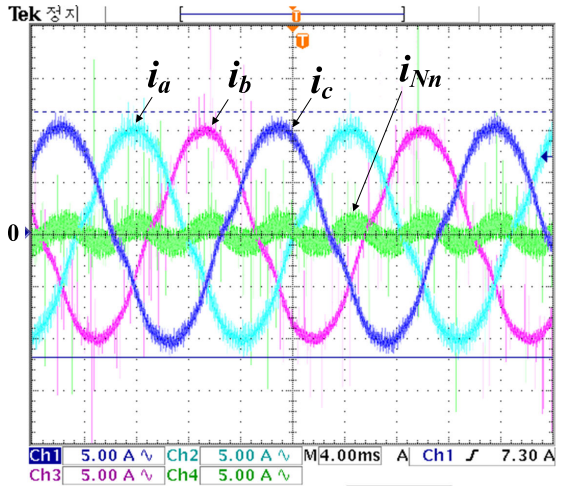

(a)

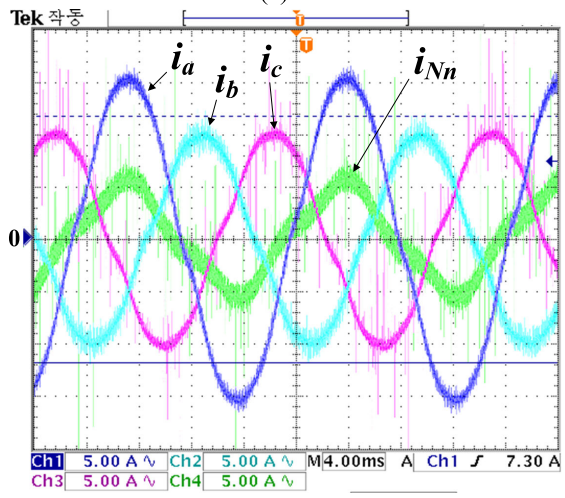

(b)

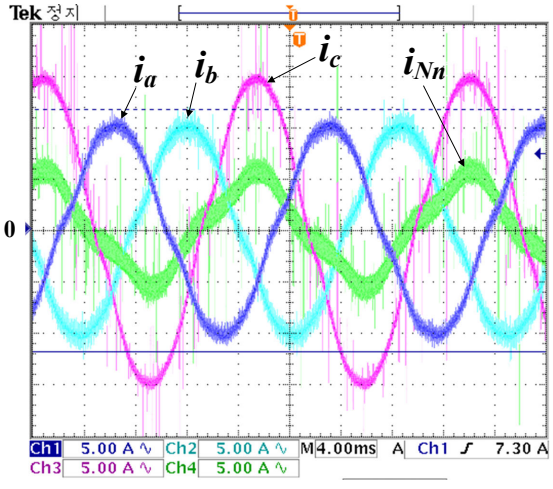

(c)

FIGURE 12. Experimental results of the output phase current of the inverter and neutral line current, (a) at balanced condition of the grid (r:s:t = 1:1:1), (b) when applying the reactive compensation at the unbalanced condition (r:s:t = 1.5:1:1), (c) when applying the effective compensation at the unbalanced condition (r:s:t = 1:1:1.5).

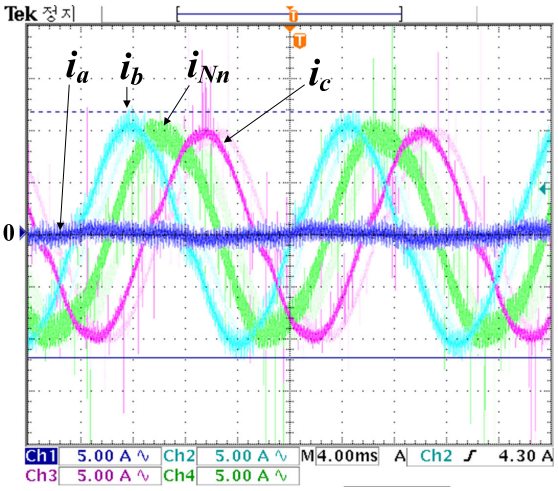

(a)

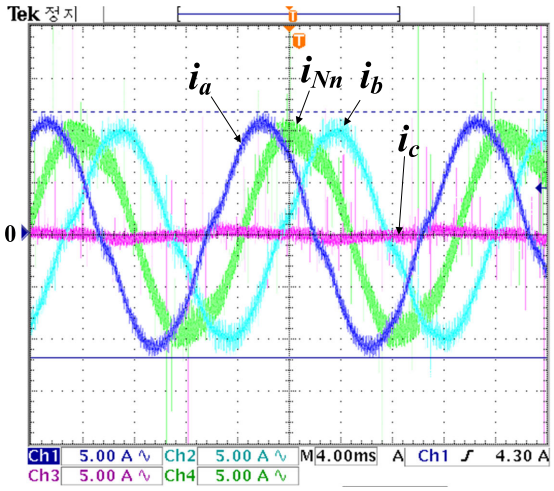

(b)

FIGURE 13. Experimental waveform of the inverter output current and neutral line current at extremely unbalanced condition of the grid current, (a) with reactive compensation when the *a*-phase current is zero, (b) with effective compensation when the *c*-phase current is zero.

of *c*-phase current (i_c) is larger than other *a*- and *b*-phases (i_a and i_b), indicating that each phase of the inverter outputs an unbalanced current. It can be seen that the unbalanced current flows through the neutral line (i_{Nn}) and is in-phase with the *c*-phase current (i_c) of the inverter.

Fig. 13(a) is an experimental waveform at extremely unbalanced condition of the grid current when applying the reactive compensation. Here, the output current of *a*-phase of the inverter is zero. In this case, the *a*-phase current is 0.0A and the peak of *b*-phase and *c*-phase current are 10.0A, respectively, indicating that the unbalanced current is output from the inverter and flows through the neutral line (i_{Nn}). Fig. 13(b) is an experimental result of the output current of the inverter *c*-phase being 0A with applying the effective compensation. The output current of the other two phases flows through the neutral line with a peak value of 10A.

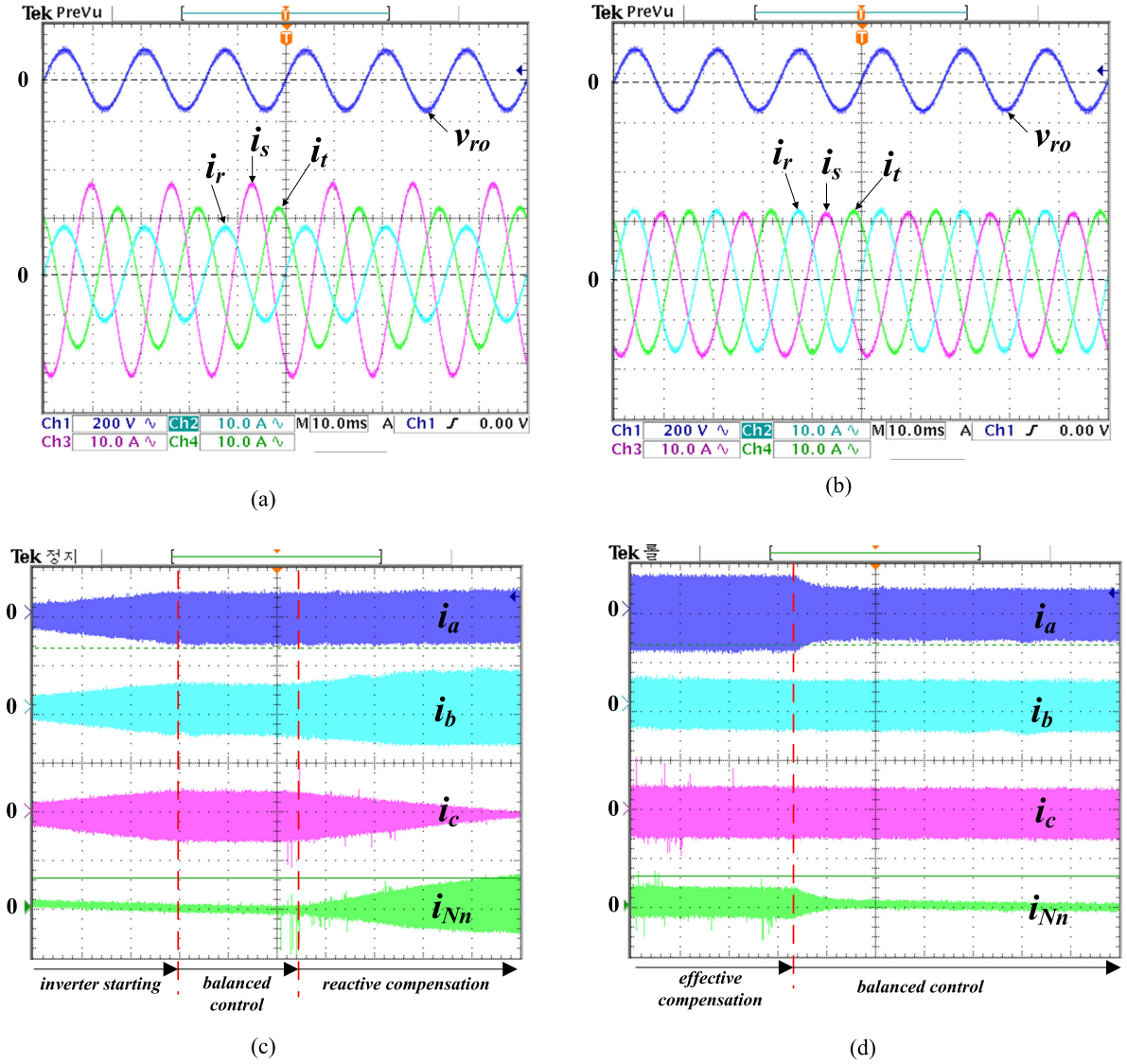

FIGURE 14. Experimental results of the proposed imbalance compensation algorithms, (a) Before applying compensation algorithm with unbalanced grid currents, (b) After applying the reactive compensation, (c) the process by which the imbalance compensation algorithms are applied, (d) vice versa of (c).

Fig. 14(a) shows the r-phase voltage (v_{ro}) of the grid and each phase current (i_r, i_s, i_t) of the grid at 15% imbalance rate of the grid current. In this case, r-phase current of the grid is 7.1A, s-phase is 14.1A, and t-phase 10.6A in rms. Fig. 14(b) is the r-phase voltage (v_{ro}) of the grid and each phase current (i_r, i_s, i_t) of the grid after applying the reactive compensation. We can notice that each phase current of the grid is balanced at 10.6A and that the imbalance rate of the grid current decreases compared to Fig. 14(a).

When the grid current has an imbalance, the control algorithm drives the reactive compensation algorithm first. If ESS has sufficient energy, or if the imbalance rate increases and the reactive compensation is insufficient, the effective power is delivered directly to the grid through the effective compensation algorithm to compensate for the imbalance of the grid current. Fig. 14(c) and (d) represent the process by which the proposed compensation algorithms are applied through each output phase current of the inverter and neutral line current. When the inverter starts operating, it first outputs a constant current. When the compensation algorithm is applied, the inverter starts to control for each phase current of the inverter. The b-phase output increases current for the effective compensation, and the c-phase output current decreases. The current flowing on the neutral line can be seen to increase in amplitude with applying the effective compensation algorithm.

In terms of reliability, it would be said that the 3-leg inverter, which has small number of parts and employs a Δ-Y transformer having low failure rate, is the best. However, the failure rate of the overall system is significantly affected by the number of switching devices having high failure rate, resulting in a similar failure rate to split dc-link capacitor

3-leg inverter. Furthermore, 4-leg inverters, which require many numbers of switching devices having high failure rate, are relatively unfavorable, but show the highest reliability when switching using the redundancy effect is applied [17].

Since 2005, the NFPA's (National Fire Protection Association) NEC (National Electrical Code) allows transformer-less (or non-galvanically) inverters for grid-connection. The VDE 0126-1-1 and IEC 6210 also have been amended to allow and define the safety mechanisms needed for such systems. Currently, grid-connected inverters employ many non-isolated inverters. According to IEC regulations (IEC 62109), it does not require the use of transformers to satisfy galvanic isolation. There is no problem with grid-connection as long as the dc component is complied with the dc injection regulations. The grid-connected inverter shall not inject DC current greater than 1 % of the rated inverter output current, into the utility AC interface under any operating condition [41].

The proposed hardware modification requires a component cost of approximately 267 USD as one neutral inductor and two ac capacitors are added to the previously installed 3-leg inverter. If replaced with a 4-leg inverter, it will cost about 10 times more [17]. Furthermore, the replacement of the Δ-Y transformer to meet the increased power capacity in preinstalled system can also be expected to increase the cost than the proposed method.

Clearly, we agree that the utilization of Δ-Y transformer, which has a sufficient power capacity to be capable of flowing the unbalanced current, would be superior in terms of reliability when it is a new installation. Nevertheless, we argue that split dc-link capacitor 3-leg inverter is a good alternative if the load imbalance increases in a previously installed 3-leg inverter system.

IV. CONCLUSION

In this paper, we proposed two kinds of compensation algorithms that can improve the imbalance rate of the grid current using the reactive and effective power of the grid and the load. The reactive compensation improves the imbalance rate of the grid current with minimum power of the dc-link of the inverter. The effective compensation directly supplies the effective power to the grid for compensating the imbalance of the grid current. To verify the validity and performance of the proposed compensation algorithm, it is applied the split dc-link capacitor 3-leg inverter with a power calculator board.

In conclusion, we confirm that even the previously installed 3-leg inverter system can reduce the imbalance rate of the grid current through minimal structural modifications and control algorithm changes. By applying the proposed approach, we believe that there will be a great effect on improving the imbalance rate of the grid.

REFERENCES

[1] F.-J. Lin, K.-H. Tan, Y.-K. Lai, and W.-C. Luo, "Intelligent PV power system with unbalanced current compensation using CFNN-AMF," *IEEE Trans. Power Electron.*, vol. 34, no. 9, pp. 8588–8598, Sep. 2019.

[2] M. J. H. Moghaddam, A. Kalam, M. R. Miveh, A. Naderipour, F. H. Gandoman, A. A. Ghadimi, and Z. Abdul-Malek, "Improved voltage unbalance and harmonics compensation control strategy for an isolated microgrid," *Energies*, vol. 11, no. 10, pp. 2688–2714, Oct. 2018.

[3] K. Jung and Y. Suh, "Analysis and control of neutral-point deviation in three-level NPC converter under unbalanced three-phase AC grid," *IEEE Trans. Ind. Appl.*, vol. 55, no. 5, pp. 4944–4955, Sep. 2019.

[4] P. J. Douglass, I. Trintis, and S. Munk-Nielsen, "Voltage unbalance compensation with smart three-phase loads," in *Proc. Power Syst. Comput. Conf. (PSCC)*, Jun. 2016, pp. 1–7.

[5] J. Hu, X. Fu, T. Liao, X. Chen, K. Ji, H. Sheng, and W. Zhao, "Low voltage distribution network line loss calculation based on the theory of three-phase unbalanced load," in *Proc. the 3rd Int. Conf. Intell. Energy Power Syst., (IEPS)*, Hangzhou, China, Oct. 2017, pp. 65–71.

[6] J. Han, Y. S. Oh, G. H. Gwon, D. U. Kim, C. H. Noh, T. H. Jung, S. J. Lee, and C. H. Kim, "Modeling and analysis of a low-voltage DC distribution system," *Resources*, vol. 4, no. 3, pp. 713–735, Sep. 2015.

[7] J. Wang, D. D. Konikkara, and A. Monti, "A generalized approach for harmonics and unbalanced current compensation through inverter interfaced distributed generator," in *Proc. IEEE 5th Int. Symp. Power Electron. Distrib. Gener. Syst. (PEDG)*, Jun. 2014, pp. 1–8.

[8] S.-P. Kim, S.-G. Song, S.-J. Park, and F.-S. Kang, "Output voltage unbalance compensation using offset voltage of neutral point in 3-phase 3-leg inverter employing split dc-link capacitor," *Electronics*, vol. 10, no. 9, p. 1029, 2021.

[9] *IEEE Standard Test Procedure for Polyphase Induction Motors and Generators*, Standard 112-1996, 1991. [Online]. Available: https://ieeexplore.ieee.org/document/210975

[10] *IEEE Recommended Practice for Monitoring Electric Power Quality*, Standard 1159-2019, Aug. 2019. [Online]. Available: https://ieeexplore.ieee.org/document/8796486

[11] *IEEE Recommended Practice for Excitation System Models for Power System Stability Studies*, Standard 421.5-2015, 2016. [Online]. Available: http://home.engineering.iastate.edu/~jdm/ee554/IEEEstd421.5-016RecPracExSysModsPwrSysStabStudies.pdf

[12] D. Soto, C. Edrington, S. Balathandayuthapani, and S. Ryster, "Voltage balancing of islanded microgrids using a time-domain technique," *Electr. Power Syst. Res.*, vol. 84, no. 1, pp. 214–223, Mar. 2012.

[13] P. K. Goel, B. Singh, S. S. Murthy, and N. Kishore, "Isolated wind–hydro hybrid system using cage generators and battery storage," *IEEE Trans. Ind. Electron.*, vol. 58, no. 4, pp. 1141–1153, Apr. 2011.

[14] R. Aboelsaud, A. Ibrahim, and A. G. Garganeev, "Review of three-phase inverters control for unbalanced load compensation," *Int. J. Power Elect. Drive Syst.*, vol. 10, no. 1, pp. 242–255, 2019.

[15] A. Hintz, U. R. Prasanna, and K. Rajashekara, "Comparative study of the three-phase grid-connected inverter sharing unbalanced three-phase and/or single-phase systems," *IEEE Trans. Ind. Appl.*, vol. 52, no. 6, pp. 5156–5164, Nov. 2016.

[16] V. Khadkikar and A. Chandra, "An independent control approach for three-phase four-wire shunt active filter based on three H-bridge topology under unbalanced load conditions," in *Proc. IEEE Power Electron. Spec. Conf.*, Jun. 2008, pp. 4643–4649.

[17] Y.-G. Kwak, D.-H. Heo, S.-P. Kim, S.-G. Song, S.-J. Park, and F.-S. Kang, "Reliability and economic efficiency analysis of 4-leg inverter compared with 3-leg inverters," *Electronics*, vol. 10, no. 1, p. 87, Jan. 2021.

[18] J. Weidong, X. Zhang, W. Wang, J. Wang, F. Zhai, J. Li, and L. Li, "A novel modulation strategy with unconditional neutral point voltage balance and three switching actions in one switching cycle for neutral point clamped three-level converter," *IEEE Trans. Ind. Electron.*, vol. 66, no. 7, pp. 5025–5038, Jul. 2019.

[19] W.-H. Choi, C.-S. Lam, M.-C. Wong, and Y.-D. Han, "Analysis of DC-link voltage controls in three-phase four-wire hybrid active power filters," *IEEE Trans. Power Electron.*, vol. 28, no. 5, pp. 2180–2191, May 2013.

[20] G. Dong and O. Ojo, "Current regulation in four-leg voltage-source converters," *IEEE Trans. Ind. Electron.*, vol. 54, no. 4, pp. 2095–2105, Aug. 2007.

[21] Z. Lin, X. Ruan, L. Jia, W. Zhao, H. Liu, and P. Rao, "Optimized design of the neutral inductor and filter inductors in three-phase four-wire inverter with split DC-link capacitors," *IEEE Trans. Power Electron.*, vol. 34, no. 1, pp. 247–262, Jan. 2019.

[22] Z. Liu, J. Liu, and J. Li, "Modeling, analysis, and mitigation of load neutral point voltage for three-phase four-leg inverter," *IEEE Trans. Ind. Electron.*, vol. 60, no. 5, pp. 2010–2021, May 2013.

[23] S. Y. Kim, S. G. Song, and S. J. Park, "Minimum loss discontinuous pulse-width modulation per phase method for three-phase four-leg inverter," *IEEE Access*, vol. 8, pp. 122923–122935, 2020.

[24] S.-J. Chee, S. Ko, H.-S. Kim, and S.-K. Sul, "Common-mode voltage reduction of three-level four-leg PWM converter," *IEEE Trans. Ind. Appl.*, vol. 51, no. 5, pp. 4006–4016, Sep. 2015.

[25] N.-Y. Dai, M.-C. Wong, F. Ng, and Y.-D. Han, "A FPGA-based generalized pulse width modulator for three-leg center-split and four-leg voltage source inverters," *IEEE Trans. Power Electron.*, vol. 23, no. 3, pp. 1472–1484, May 2008.

[26] J.-H. Kim and S.-K. Sul, "A carrier-based PWM method for three-phase four-leg voltage source converters," *IEEE Trans. Power Electron.*, vol. 19, no. 1, pp. 66–75, Jan. 2004.

[27] J. H. Kim, S. K. Sul, H. Kim, and J. K. Ji, "A PWM strategy for four-leg voltage source converters and applications to a novel line interactive UPS in a three phase four wire system," in *Proc. 39th IEEE Ind. Appl. Conf. (IAS)*, Seattle, WA, USA, Oct. 2004, pp. 2202–2209.

[28] A. Videt, P. Le Moigne, N. Idir, P. Baudesson, and X. Cimetiere, "A new carrier-based PWM providing Common-Mode-Current reduction and DC-bus balancing for three-level inverters," *IEEE Trans. Ind. Electron.*, vol. 54, no. 6, pp. 3001–3011, Dec. 2007.

[29] F. Li, F. He, Z. Ye, T. Fernando, X. Wang, and X. Zhang, "A simplified PWM strategy for three-level converters on three-phase four-wire active power filter," *IEEE Trans. Power Electron.*, vol. 33, no. 5, pp. 4396–4406, May 2018.

[30] M. R. Miveh, M. F. Rahmat, A. A. Ghadimi, and M. W. Mustafa, "Control techniques for three-phase four-leg voltage source inverters in autonomous microgrids: A review," *Renew. Sustain. Energy Rev.*, vol. 54, pp. 1592–1610, Feb. 2016.

[31] W. Wang, B. Zhang, and F. Xie, "A novel SVPWM for three-level NPC inverter based on m-mode controllability," *IEEE Trans. Ind. Electron.*, vol. 65, no. 8, pp. 6055–6065, Aug. 2018.

[32] R. Zhang, V. H. Prasad, D. Boroyevich, and F. C. Lee, "Three-dimensional space vector modulation for four-leg voltage-source converters," *IEEE Trans. Power Electron.*, vol. 17, no. 3, pp. 314–326, May 2002.

[33] M. Aissani and K. Aliouane, "Three-dimensional space vector modulation for four-leg voltage-source converter used as an active compensator," in *Proc. SPEEDAM*, Jun. 2010, pp. 1416–1421.

[34] H. Golwala and R. Chudamani, "New three-dimensional space vector-based switching signal generation technique without null vectors and with reduced switching losses for a grid-connected four-leg inverter," *IEEE Trans. Power Electron.*, vol. 31, no. 2, pp. 1026–1035, Feb. 2016.

[35] Q. Zhang, P. Zhang, S. Zhao, J. Gao, and X. Sun, "Research on a discontinuous three-dimensional space vector modulation strategy for the three-phase four-leg inverter," in *Proc. IEEE 8th Int. Power Electron. Motion Control Conf. (IPEMC-ECCE Asia)*, May 2016, pp. 575–580.

[36] M. Llonch-Masachs, D. Heredero-Peris, D. Montesinos-Miracle, and J. Rull-Duran, "Understanding the three and four-leg inverter space vector," in *Proc. 18th Eur. Conf. Power Electron. Appl. (EPE ECCE Eur.)*, Sep. 2016, pp. 1–10.

[37] F. Rojas, R. Kennel, R. Cardenas, R. Repenning, J. C. Clare, and M. Diaz, "A new space-vector-modulation algorithm for a three-level four-leg NPC inverter," *IEEE Trans. Energy Convers.*, vol. 32, no. 1, pp. 23–32, Mar. 2017.

[38] S. Bifaretti, A. Lidozzi, L. Solero, and F. Crescimbini, "Comparison of modulation techniques for active split DC-bus three-phase four-leg inverters," in *Proc. IEEE Energy Convers. Congr. Expo. (ECCE)*, Sep. 2014, pp. 14–18.

[39] B. Axelrod, Y. Berkovich, and A. Ioinovici, "Increasing voltage utilization in split-link," in *Proc. Int. Symp. Circuits Syst. (ISCAS)*, vol. 3, no. 6, 2003, pp. 1562–1569.

[40] M. K. Mishra, A. Joshi, and A. Ghosh, "Control schemes for equalization of capacitor voltages in neutral clamped shunt compensator," *IEEE Trans. Power Del.*, vol. 18, no. 2, pp. 538–544, Apr. 2003.

[41] *Safety of Power Converters for Use in Photovoltaic Power Systems—Part 1: General Requirements*, document IEC 62109-1, 2010.

SUN-PIL KIM received the B.S. and M.S. degrees in control and instrumentation engineering from Hanbat National University, South Korea, in 2011 and 2013, respectively, and the Ph.D. degree in electrical engineering from Chonnam National University, in 2021. Since 2021, he has been with the Energy Conversion Research Center, Korea Electronics Technology Institute (KETI), as a Postdoctoral Fellow.

SUNG-GEUN SONG (Member, IEEE) received the B.S., M.S., and Ph.D. degrees in electrical engineering from Chonnam National University, South Korea, in 1998, 2000, and 2007, respectively. Since 2007, he has been with the Energy Conversion Research Center, Korea Electronics Technology Institute (KETI), as a Principal Researcher.

SUNG-JUN PARK received the B.S., M.S., and Ph.D. degrees in electrical engineering and the Ph.D. degree in mechanical engineering from Pusan National University, Busan, South Korea, in 1991, 1993, 1996, and 2002, respectively. From 1996 to 2000, he was an Assistant Professor with the Department of Electrical Engineering, Koje College, Koje, South Korea. From 2000 to 2003, he was an Assistant Professor with the Department of Electrical Engineering, Tongmyong College, Busan. Since 2003, he has been a Professor with the Department of Electrical Engineering, Chonnam National University, Gwangju, South Korea. His research interests include power electronics, motor control, mechatronics, and micromachine automation.

FEEL-SOON KANG (Member, IEEE) received the M.S. and Ph.D. degrees in electrical engineering from Pusan National University, South Korea, in 2000 and 2003, respectively. Since 2003, he has been with the Department of Electrical Engineering, Osaka University, Japan, as a Postdoctoral Fellow. Since 2004, he has been with the Department of Electronic Engineering, Hanbat National University, South Korea, as a Professor. His research interests include power electronics, including design, control, and reliability analysis of various power conversion systems for photovoltaic power generation systems, electric vehicles, and HVDC systems. He is a member of KIEE and KIPE. He received the Student Award and the Best Presentation Prize from the IEEE Industrial Electronics Society, in 2001. He was honored with Academic Award from Pusan National University and Hanbat National University, in 2003 and 2005, respectively. He received several best paper awards from the Korean Institute of Electrical Engineers (KIEE) and the Korean Institute of Power Electronics (KIPE). He served as the Vice-Chairman for the Organizing Committee for the International Telecommunications Energy Conference (IEEE Intelec 2009), IEEE Vehicle Power and Propulsion Conference (IEEE VPPC 2012), IEEE Transportation Electrification Conference and Expo (IEEE ITEC 2016), and International Conference on Electrical Machines and Systems (ICEMS 2010, 2013, and 2018). He served as a Secretary for International Conference on Magnetically Levitated Systems and Linear Drives (Maglev 2011). He served as an Associate Editor for the IEEE TRANSACTIONS ON INDUSTRIAL ELECTRONICS, from 2004 to 2011.